2003 Pacific Conference on Earthquake Engineering

Experiment of a sliding isolated structure subjected to near-fault ground motions

L.-Y. Lu, M.-H. Shih, S.-W. Tzeng, C.-S. Chang Chien

Dept. of Construction Engineering, National Kaohsiung First University of Science and Technology, Kaohsiung, Taiwan, ROC

ABSTRACT: In this paper, the experimental results of a shaking-table test that was performed on a sliding isolated structure subjected to a near-fault and a far-field ground motions are presented and compared. In the test, a set of pulse accelerations with various pulse periods were also artificially generated and imposed on the isolated structure, in order to study the effect of the pulse wave component possessed in a near-fault earthquake. Based on the test data, several effects of near-fault earthquakes on the response of the isolated structure are investigated and discussed. These effects include the vertical ground motion, the over-turning moment of the structure and the period of the pulse wave, etc. The test results show that the pulse component in the near-fault earthquake wave can lead to an isolation motion similar to resonant response. As a result, and the isolator displacement of the sliding isolated structure is considerably amplified in the near-fault earthquake as compared with that in the far-field earthquake.

1 INTRODUCTION

The technology of seismic isolation has been developed to protect civil engineering structures from seismic hazard for decades. Design codes for seismic isolation have also been developed in many countries (Naeim and Kelly 1999). Presently, there are thousands of base isolated structures constructed worldwide (Fujita 1998, Martelli 1998). Some of these constructions were even subjected to real-life earthquakes and proved that the technology is effective in mitigating seismic responses of structural systems (Kelly 1998). However, there are very few structures actually subjected to near-fault earthquakes that possess very different wave characteristics from those of usual far-field earthquakes. Also, there are relatively few experimental studies on the dynamic responses of near-fault seismic isolation; therefore, the problem of near-fault isolation remains inconclusive.

According to the literature and the records of the 1999 Chi-Chi earthquake (Taiwan), it is observed that near-fault earthquakes usually have the following features (Hall et al. 1995, Chai and Loh 2000): (1) a high level of peak ground acceleration, (2) a large vertical ground motion, (3) a long-period pulse-like waveform, especially in velocity field. The pulse-wave component, whose pulse period usually ranges from 2 ~ 4 seconds, can be very destructive to soft structural systems of long vibration periods. The reason that the Chi-Chi earthquake seriously damaged many structures near the fault can be due to the combination of these three features.

Seismic isolation systems using sliding bearings have been recognized as one of practical and effective isolation methods. By implementing sliding supports under the base of the isolated structure, the transmitted seismic forces from the ground to the structure can be reduced to a level equal to the total friction forces of the bearings (Lu and Yang 1997). Friction pendulum system (FPS) is one famous example of sliding isolation systems (Mokha 1991) and has been implemented in many existing structures. In a friction pendulum system, the friction mechanical behaviour between the slider and the spherical sliding surface governs the global seismic response of the isolation system. Depending on the friction material used, the friction coefficient of the sliding interface of a FPS can be a function

of the sliding velocity and/or the normal compression stress applied on the sliding interface. Furthermore, when a FPS isolated structure is subjected to a near-fault ground motion, the features of the ground motions mentioned above might further complicate the behaviour of the sliding isolated structure. Especially, the vertical component of the ground motion and the overturning moment of the superstructure may greatly influence the normal compression force of the isolators and also change the friction force of the isolators.

In this study, a shaking table test has been conducted on a rigid structure isolated by a friction pendulum system, so the difference in the dynamic behaviour of the sliding isolation system subject to near-fault and far-field earthquakes can be experimentally investigated and compared. An isolator element test was also performed prior to the shaking table test, in order to obtain the frictional property of the isolators used in the test. The result of element test is also shown in this paper.

2 PROPERTIES OF FPS ISOLATORS

2.1 Element Test for FPS Isolators

Several FPS isolators were fabricated for the shaking table test program. For each isolator, the maximum design isolator drift is ± 150mm. The radius of the curvature of the sliding spherical surface is 560mm, which gives an isolation period of 1.5 second. The slider of each isolator is composed of plastic-polymer material, which has very good compressibility and ductility in shear. In order to fully understand the frictional property of the isolators, an isolator element test was performed independently before the shaking table test. The purpose of the element test was to quantify the influence of sliding velocity and compression stresses on the friction coefficient of the isolator. The set-up for the isolator element test is shown in Figure 1. Also, in order to simulate the vertical dead load, a hydraulic actuator was placed vertically to apply a vertical compression force (ranging from 10 to 100 kN) on the isolator specimen. A dynamic actuator was placed horizontally to apply a horizontal shear force on the tested isolator. The horizontal load is periodical and has a triangular loading pattern with different loading frequencies, which can generate different constant sliding velocities.

2.2 Results of Isolator Element Test

Figures 2 and 3 show the friction coefficient of the isolator as a function of the compression stress and the sliding velocity, respectively. From the figures, it is observed that the friction coefficient is insensitive to the variation of the sliding velocity, but the coefficient greatly depends on the compression stress. As shown in Figure 3, the friction coefficient decreases from 0.16 to 0.02 as the compression stress increases from 10 to 82 N/mm^2. This implies that when the FPS is installed on a structure, a variation on the column axial force may greatly influence the friction force and the dynamic behaviour of the FPS isolators.

3 SHAKING TABLE TEST PROGRAM

3.1 Test Setup

The shaking table test was conducted in the earthquake simulation laboratory of the National Center for Research on Earthquake Engineering (NCREE), Taipei, Taiwan. The test setup and the instrumentation are shown in Figures 4 and 5. The test structure is an assembly of several layers of mass blocks. The mass blocks are connected to each other by vertical tension rods at the four corners of the blocks. The total mass and height of the structure can be adjusted by changing the number of the blocks. The structure has very high rigidity and can be considered as a rigid block. The reason of using such a rigid structure is that the focus of the present study is on the behavior of the isolation system, not on the dynamic response of the super-structures. Furthermore, in order to investigate the effect of overturning moments, two type of the structures with different number of layers were used in the test: (A) structure with three block layers (see Figure 4); (B) structure with five block layers (see Figure 5). The detail information about each structure type is listed in Table 1.

A FPS isolator is mounted on each of the four legs of the test structure (see Figure 6). A tri-axial load cell was mounted between each column base plate and the isolator, in order to measure the column axial force and the isolator shear forces (friction forces) in two orthogonal directions. Accelerometers and displacement sensors (LVDT) were placed on the top and base of the rigid block and also on the shaking table (see Figure 4), in order to measure the response of the isolated structure.

Table 1 Structures Types Used in the Shaking Table Test

Structure Type	No. of Layers	Weight (ton)	Height (mm)	Height of Mass Center (mm)	Ave. Slider Compression (N/mm^2)	Estimated Friction Coeff.
A	3	16.4	1621	1081	41.81	0.062
B	5	18.4	2421	1881	46.91	0.053

3.2 **Input Ground Motions**

In the shaking table test, two sets of earthquake records measured at the same station TCU075 (Taiwan) were used as the input ground accelerations, therefore the two records have the same soil condition. The first record was obtained in the Chi-Chi earthquake that severely damaged central Taiwan in September of 1999. Figures 7(a) and 7(b) depict the horizontal and vertical acceleration components of this record. Since the station TCU075 is located only 0.43 km away from the ruptured fault of Chi-Chi earthquake, the record set in Figure 7 represents a near-fault ground motion. The ground accelerations of the second record set shown in Figures 8(a) and 8(b) represent a far-field earthquake. This ground motion was recorded earlier by station TCU075 in an earthquake whose epicenter was located more than one hundred kilometers away. It must be mentioned that in order to compare the isolation behaviour under different earthquake intensities, the peak ground accelerations (PGA) of these records were adjusted from low to high levels in the test.

Comparing Figures 7 and 8, it is observed that the near-fault earthquake has a pulse-like waveform between the 5th to 15th seconds, while the far-field earthquake contains high-frequency components. Makris and Chang (2000) classified near-fault earthquakes into three types named A, B and C types, depending on the number of pulses appearing in the waveform. They also proposed simple trigonometric functions to approximate near-fault seismic waves. The earthquake shown in Figure 7 may be classified as type B with a pulse period T_p about 4 seconds. The time histories of ground acceleration and velocity of a type B pulse wave can be approximated by

$$\ddot{u}_g(t) = w_p \frac{n_p}{2} \sin(w_p t) \tag{1}$$

$$\dot{u}_g(t) = \frac{n_p}{2} - \frac{n_p}{2} \cos(w_p t), \qquad 0 \le t \le T_p, \qquad w_p = \frac{2p}{T_p} \tag{2}$$

where w_p and T_p are the frequency and period of the pulse; v_p is the amplitude of the pulse in the velocity field.

4 **TEST RESULTS**

4.1 **Comparison of Near-Fault and Far-Field Responses with Different PGA**

Figures 9 and 10 compare, respectively, the maximum isolator drift and structure acceleration of the 3-layer structure (type A) subjected to the horizontal components of TUC075 near-fault and far-field acceleration records. It is observed that the isolator drift is considerably amplified in the near-fault earthquake as the PGA level increases, while the structural acceleration is not affected much. This implies that a FPS system in a near-fault earthquake may be still effective for acceleration mitigation, but isolators with extremely large diameter may be required to accommodate the large isolator drift.

4.2 **Effect of Pulse Period**

The theoretical study by Lu *et al.* (2002) has shown that in the long-period pulse of a near-fault earthquake is the main cause that amplifies the isolator drift of a sliding isolated structure. On the other hand, as mentioned above, the pulse wave component in a near-fault earthquake usually can be approximated by a simple trigonometric function. In this study, a pulse ground acceleration approximated by Equation (1) was imposed on the isolated 3-layer structure (type A), in order to study the pulse effect. The pulse period T_p was changed from 1.00 to 1.625 seconds in the test. Figures 11 and 12 show that both isolator drift and structural acceleration are amplified around the isolator period 1.5 second. This means that even though strictly speaking the pulse excitation is not a harmonic one, a resonance phenomenon is still observed around the fundamental period of the isolated structure. Furthermore, a close investigation of Figures 11 and 12 reveals that if the response of T_p = 1.00 second is used as a reference value, the amplification factor for the isolator drift is around 90%, while for the structural acceleration the factor is around 50%. This implies that the pulse is more influential to the isolator drift. With the pulse PGA scaled to 200 gal and pulse period set to T_p = 1.50 second, Figures 13 and 14 depict the time histories of the structural acceleration and isolator drift of the structure subjected to the type-B pulse wave.

4.3 **Effect of Over-Turning Moment**

Generally speaking, the over-turning moment of a structure induced by a horizontal ground motion is proportional to the height of the structure. The over-turning moment will cause variation of the column axial forces and produce a tendency of rocking motion. In a sliding isolated structure, the variation of the column forces have two effects on the isolators: (1) it changes the normal compression force applied on the isolator sliding surface, (2) it changes the friction coefficient of the isolators, if the coefficient is sensitive to the normal force such as the one shown in Figure 3. Nevertheless, both above effects can change the sliding friction forces (shear force) of the isolators. In order to study the influence of the over-turning moment, the two types of the structures with different structural heights described in Table 1 were tested.

For the far-field earthquake, Figures 15 and 16 show, respectively, the maximum isolator drift and structural acceleration for both 3-layer (type A) and 5-layer (type B) structures. On the other hand, Figures 17 and 18 compare the same maximum response values for the near-fault earthquake. From these four figures, it is observed that in the near-fault earthquake the over-turning moment produces a significant increase on the isolator drift, but has relatively less effect on the acceleration response. When the structure is subjected to the near-fault earthquake, Figures 19 and 20 show the time histories of the axial forces of the northwest-corner isolator of the 3-layer and 5-layer structures, respectively. It is shown that the 5-layer structure has an axial force variation about 70% of the dead load, while the variation is about 50% for the 3-layer structure.

4.4 **Effect of Vertical Ground Motion**

When both the vertical and horizontal components of the near-fault earthquake (see Figures 7(a) and 7(b)) were imposed on the isolated 3-layer structure (type A), the maximum structural responses are shown in Figures 21 and 22. Note that in these figures: (1) the PGA of the vertical component has been scaled up to be 100% of the horizontal PGA, (2) a dotted line represents the response without the vertical ground acceleration. As observed, the vertical ground acceleration has an advantage of decreasing the isolator drift but at the same time it significantly increases the structural acceleration. Because the normal compression force of an isolator is equal to the structural dead load plus the vertical ground acceleration times the structural mass, the large vertical acceleration that accompanies a near-fault earthquake can significantly increase the compression force and also the friction force of the isolator. As a result, the increased friction force reduces the isolator drift and also degrades the effectiveness of the seismic isolation.

5 **CONCLUSIONS**

In this study, an FPS isolator test and a shaking table test were performed in order to investigate the effects of near-fault ground motions on a sliding isolated structure. The isolator test shows that the friction coefficient of the isolators used in the test is insensitive to the variation of the sliding velocity, but is a function of the compression stress applied on the sliding surface. On the other hand, the results of the shaking table test demonstrate that the isolator displacement of a sliding isolated structure may be considerably amplified in a near-fault earthquake as the PGA level of the earthquake increases, while the transmitted acceleration up to the super-structure can still be mitigated. As shown by the test data, this behaviour can be due to the pulse-wave component possessed in the near-fault earthquake, which can induce an isolation motion similar to resonant response and amplify the isolator displacement. It is also observed in the experiment that the over-turning moment and the vertical ground acceleration are influential to the isolator drift because these two effects can considerably vary the axial compression forces and also the friction forces of the isolators.

6 **ACKNOWLEDGMENT**

This research was sponsored in part by the National Science Council, Taipei, Taiwan, R.O.C., through Grant No. 91-2211-E-327-005. The authors are grateful to the National Center for Research on Earthquake Engineering (NCREE), Taipei, Taiwan, for performing the shaking table test.

REFERENCES:

Chai, J.-F. & Loh, C.-H. 2000. Near-fault ground motion and its effect on civil structures, *International workshop on mitigation of seismic effects on transportation structures*, July 12-14, Taipei, Taiwan, R.O.C. 70-81.

Fujita, T. 1998. Seismic isolation of civil buildings in Japan, *Progress in Structural Engineering and Materials*, Vol 1(3), 295-300.

Hall, J. F, Heaton, T. H., Halling, M. W., and Wald, D. J. 1995. Near-source ground motions and its effects on flexible buildings, *Earthquake Spectra*, Vol 11, 569-605.

Kelly, J. M., 1998. Seismic isolation of civil buildings in USA, *Progress in Structural Engineering and Materials*, Vol 1(3), 279-285.

Lu, L.-Y. & Yang, Y.-B. 1997. Dynamic Response of Equipment in Structures with Sliding Support, *Earthquake Engineering and Structural Dynamics*, Vol 26(1), 61-76.

Lu, L.-Y., Shih, M.-H., Chang Chien, C.-S., and Chang, W.-N. 2002. Seismic performance of sliding isolated structures in near-fault areas, *The 7th US National Conference on Earthquake Engineering*, July 21-25, Boston, MA, USA. Session AT-2.

Makris, N. & Chang, S.-P. 2000. Effect of viscous, visoplastic and friction damping on the response of seismic isolated structures, *Earthquake Engineering and Structural Dynamics*, Vol 29, 85-107.

Martelli, A. & Forni, M. 1998. Seismic isolation of civil buildings in Europe. *Progress in Structural Engineering and Materials*, Vol 1(3), 286-294.

Mokha, A., Constantinous, M. C., Reinhorn, A. M. and Zayas, V. A. 1991. Experimental study of friction-pendulum isolation system, *J. of Structural Engineering, ASCE*, Vol (4), 1201-1217.

Naeim, F. & Kelly, J. M. 1999. Design of Seismic Isolated Structures: from theory to practice. *John Wiley & Sons.*

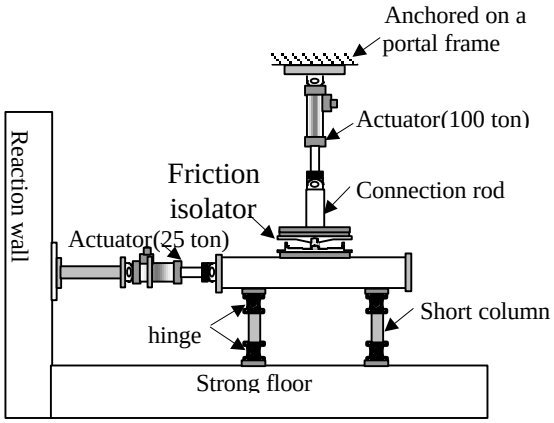

Figure 1 Isolator element test

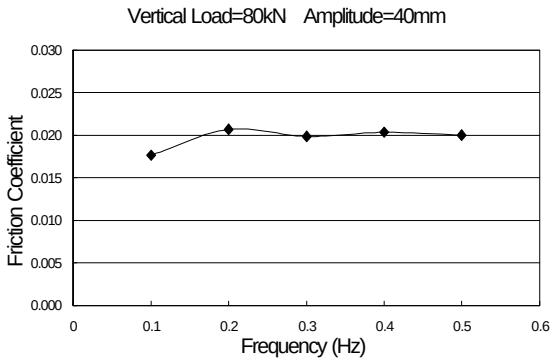

Figure 2 Friction coefficient vs. sliding velocity

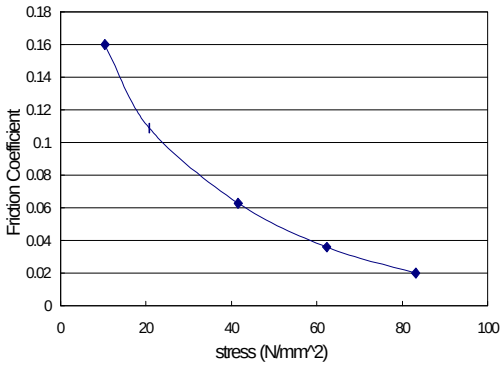

Figure 3 Friction coefficient vs. compression stress

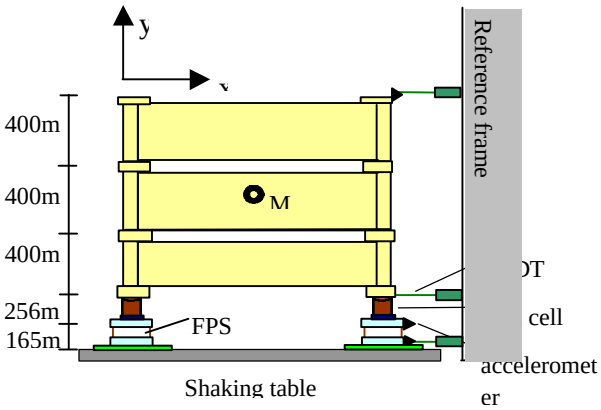

Figure 4 Set-up of shaking table test

Figure 5 Shaking table test for 5-layer structure

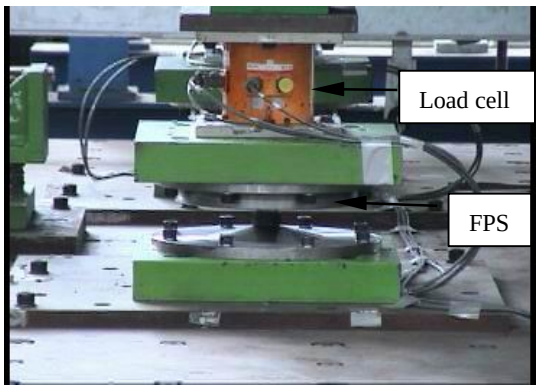

Figure 6 Photo of FPS isolator and load cell

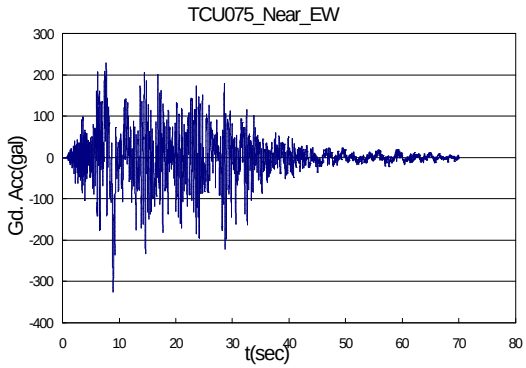

Figure 7(a) TCU075 near-fault ground acc. (horizontal)

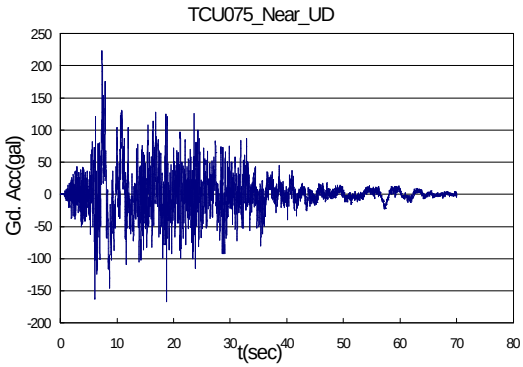

Figure 7(b) TCU075 near-fault ground acc. (vertical)

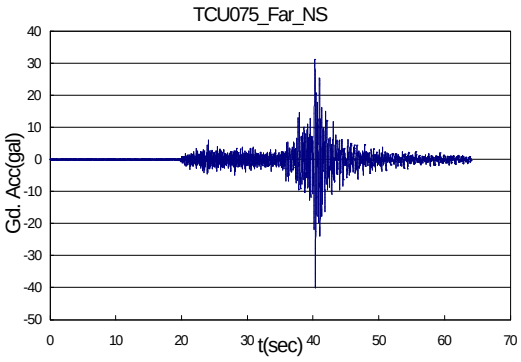

Figure 8(a) TCU075 far-field ground acc. (horizontal)

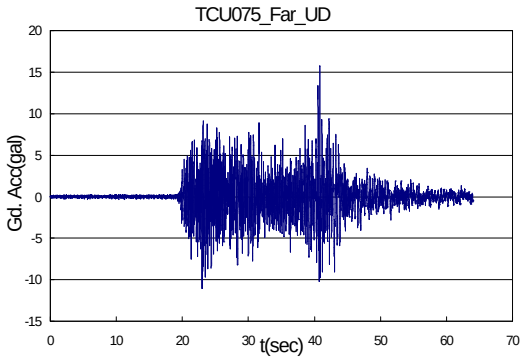

Figure 8(b) TCU075 far-field ground acc. (vertical)

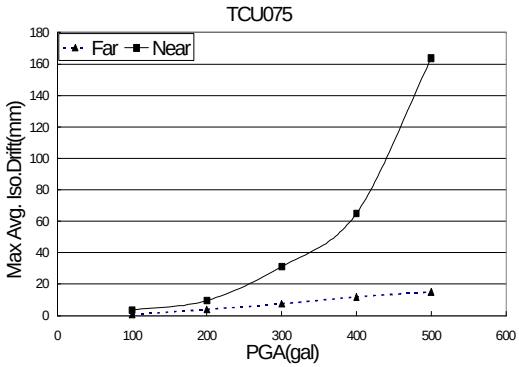

Figure 9 Maximum isolator drifts vs. PGA level

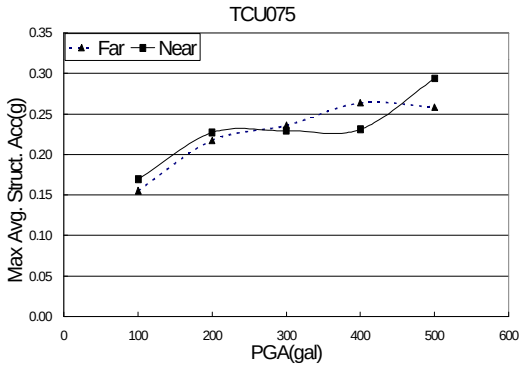

Figure 10 Maximum structural acc. vs. PGA level

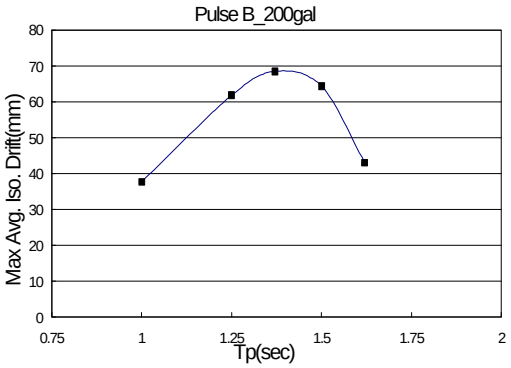

Figure 11 Maximum isolator drift vs. pulse period

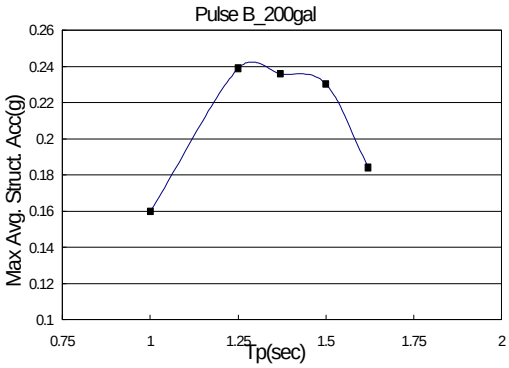

Figure 12 Maximum structural acc. vs. pulse period

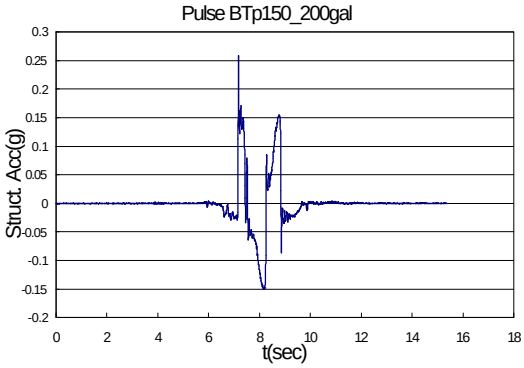

Figure 13 Structural acc. due to type-B pulse wave

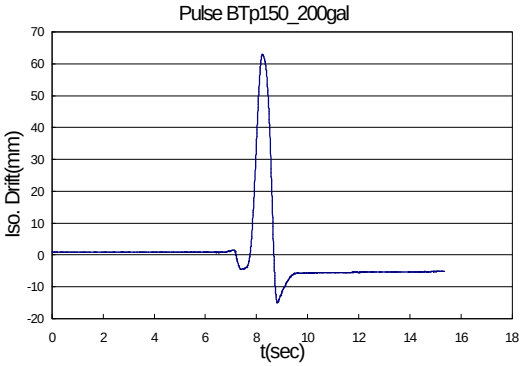

Figure 14 Isolator drift due to type-B pulse wave

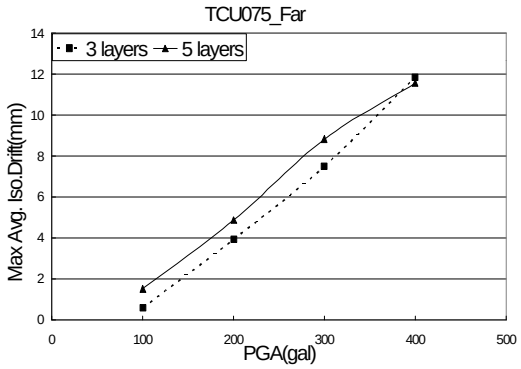

Figure 15 Far-field maximum isolator drifts

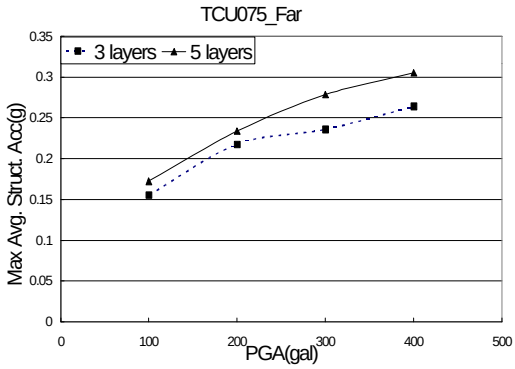

Figure 16 Far-field maximum structural accelerations

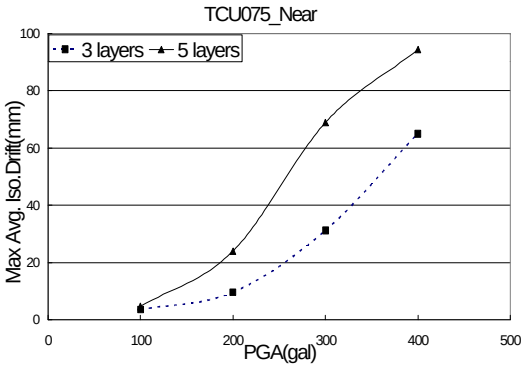

Figure 17 Near-fault maximum isolator drifts

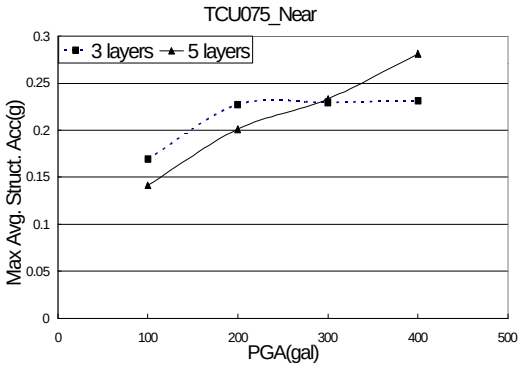

Figure 18 Near-fault maximum structural accelerations

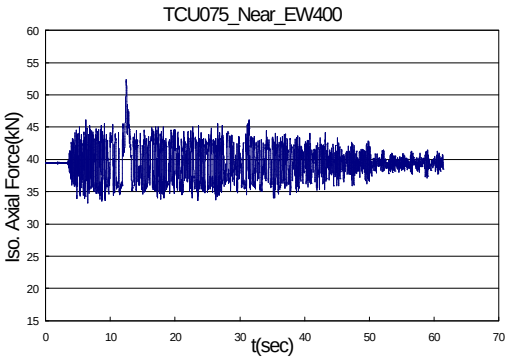

Figure 19 Axial force of isolator for 3-layer structure

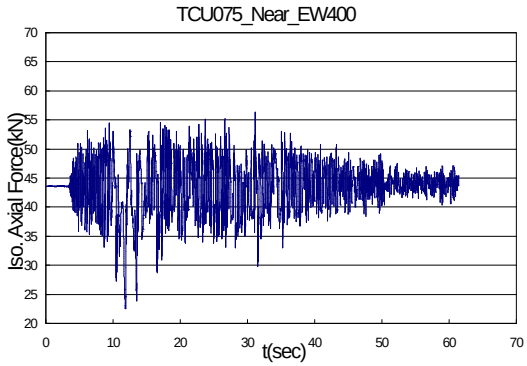

Figure 20 Axial force of isolator for 5-layer structure

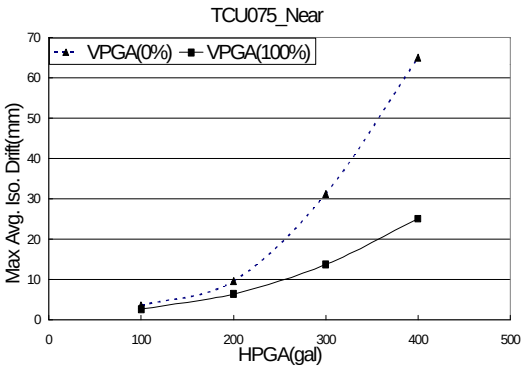

Figure 21 Maximum isolator drifts vs. PGA level

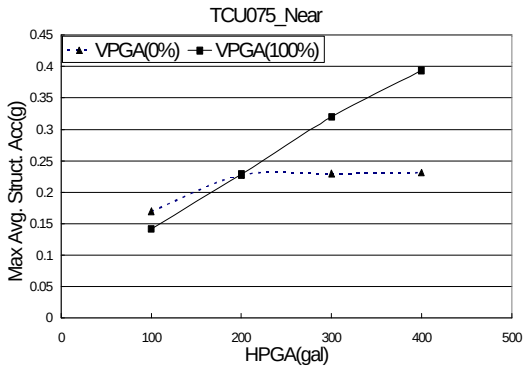

Figure 22 Maximum structural acc. vs. PGA level